

RemoteReasoner: Towards Unifying Geospatial Reasoning Workflow

Liang Yao^{1,2}, Fan Liu¹, Hongbo Lu², Chuanyi Zhang¹, Rui Min¹,
Shengxiang Xu³, Shimin Di³, and Pai Peng²

¹Hohai University, ²COWAROBOT Co. Ltd., ³Southeast University

Remote sensing imagery presents vast, inherently unstructured spatial data, necessitating sophisticated reasoning to interpret complex user intents and contextual relationships beyond simple recognition tasks. In this paper, we aim to construct an Earth observation workflow to handle complex queries by reasoning about spatial context and user intent. As a reasoning workflow, it should autonomously explore and construct its own inference paths, rather than being confined to predefined ground-truth sequences. Ideally, its architecture ought to be unified yet generalized, possessing capabilities to perform diverse reasoning tasks through one model without requiring additional fine-tuning. Existing remote sensing approaches rely on supervised fine-tuning paradigms and task-specific heads, limiting both autonomous reasoning and unified generalization. To this end, we propose RemoteReasoner, a unified workflow for geospatial reasoning. The design of RemoteReasoner integrates a multi-modal large language model (MLLM) for interpreting user instructions and localizing targets, together with task transformation strategies that enable multi-granularity tasks, including object-, region-, and pixel-level. In contrast to existing methods, our framework is trained with reinforcement learning (RL) to endow the MLLM sufficient reasoning autonomy. At the inference stage, our transformation strategies enable diverse task output formats without requiring task-specific decoders or further fine-tuning. Experiments demonstrated that RemoteReasoner achieves state-of-the-art (SOTA) performance across multi-granularity reasoning tasks. Furthermore, it retains the MLLM's inherent generalization capability, demonstrating robust performance on unseen tasks and out-of-distribution categories.

Keywords: Remote sensing, Reasoning workflow, Reinforcement learning

 **Projects:** Work in progress.

 **Contact:** yaoliang@hhu.edu.cn

1. Introduction

Remote sensing analysis has evolved beyond simple object detection Zou et al. (2023), Liu et al. (2025a) or classification Adegun et al. (2023), increasingly requiring stronger capabilities to support complex real-world decision-making. Although existing approaches Yao et al. (2025b), Liu et al. (2024a) are effective for multiple tasks, they struggle to interpret nuanced user intent and infer implicit spatial relationships for intricate queries. Reasoning Jaech et al. (2024), Xu et al. (2025) bridges this gap by enabling systems to dynamically decipher the underlying goals of ambiguous or high-level instructions (e.g., "Find areas at risk of flooding near critical infrastructure after heavy rain"). Such a geospatial workflow would conveniently accommodate varied geoscience applications Zhao et al. (2024).

Numerous efforts Lai et al. (2024), Ren et al. (2024), Chen et al. (2024b) have explored reasoning tasks in the natural image domain. For instance, LISA Lai et al. (2024) utilizes multi-modal large language models (MLLMs) Carolan et al. (2024) for reasoning-driven segmentation tasks. However, these

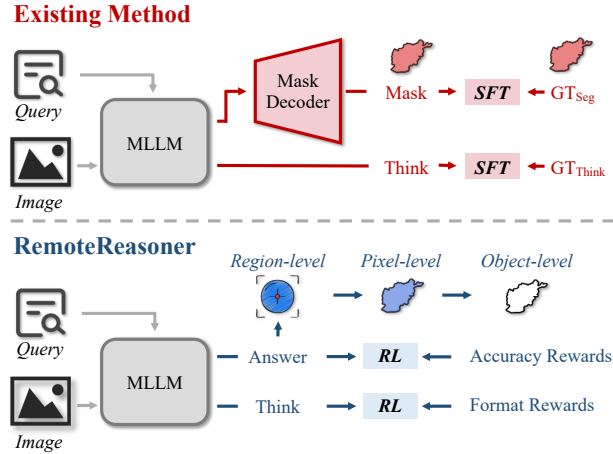


Figure 1: Comparison between Existing Frameworks and RemoteReasoner. Existing remote sensing reasoning approach (e.g., SegEarth-R1) requires SFT with annotated reasoning processes, and is limited to single-task outputs and task decoder. In contrast, our framework supports unsupervised reasoning and multi-granularity tasks.

approaches rely on supervised fine-tuning (SFT) paradigms to train the models. Such frameworks constrain model autonomy, ultimately compromising generalization capabilities. This situation can be manifested in substantial performance degradation on out-of-distribution samples and catastrophic forgetting of general capabilities Liu et al. (2025b). Similarly, the remote sensing community has seen pioneering works Li et al. (2025), Zhang et al. (2023), Wang et al. (2024). SegEarth-R1 Li et al. (2025) introduces a geospatial pixel reasoning task that integrates a hierarchical MLLM and a mask decoder to generate both reasoning processes and segmentation outputs. However, it remains constrained by SFT paradigms and exclusively supports segmentation tasks.

These limitations motivate us to design a reasoning workflow that autonomously interprets user intent through self-directed thinking. It should also efficiently generate geospatial interpretations in diverse output formats, which are tailored for various downstream intelligence analysis. Firstly, the requirement for self-thinking should be fulfilled through an open-ended learning paradigm. This aligns naturally with the emerging reinforcement learning (RL) frameworks Guo et al. (2025), Shen et al. (2025). Rather than SFT approaches that demand strictly annotated reasoning processes, RL explores the model’s self-evolution potential to cultivate reasoning capabilities. Secondly, to flexibly support multi-granularity tasks, we should avoid redundant task decoders and training through decision-level task transformation.

Followed by these insights, we propose **RemoteReasoner**, a reasoning workflow that integrates a robust MLLM and a flexible inference strategy. As shown in Fig. 1, building upon the *pixel-level* reasoning task proposed in SegEarth-R1 Li et al. (2025), RemoteReasoner further implements two novel tasks through autonomous reasoning: 1) *region-level*: geospatial region reasoning, and 2) *object-level*: geospatial contour reasoning. These three distinct tasks can be achieved through a single MLLM inference followed by a unified decision-level task transformation pipeline, significantly improving output efficiency for multi-granularity reasoning tasks.

During training, we utilize Group Relative Policy Optimization (GRPO) Shao et al. (2024) to fine-tune the reasoning model. Benefiting from our sophisticated reward function that balances output formats, localization accuracy, and quantity, RemoteReasoner demonstrates strong capabilities in

autonomous reasoning and precise *region-level* localization. This training approach maintains the inherent generalization capability of MLLM, thereby endowing it with the ability to recognize out-of-distribution categories. During inference, we design a task transformation pipeline inspired by RemoteSAM Yao et al. (2025b), which enables the model to perform *object-* and *pixel-level* reasoning tasks, eliminating redundant computations across granularities.

Extensive experimental results demonstrate that RemoteReasoner achieves state-of-the-art performance on multi-granularity reasoning tasks, evidencing its enhanced autonomous reasoning capabilities and superior generalization. For instance, RemoteReasoner achieves 3.67% accuracy improvement over SegEarth-R1 in pixel-level geospatial reasoning tasks. On unseen tasks (*e.g.*, , Referring Segmentation), our framework significantly outperforms competing models (*e.g.*, , PixelLM, LISA) in performance.

The contributions are summarized as follows:

- We propose RemoteReasoner, a unified yet generalized reasoning workflow for Earth observation, which reveals that integrating pure RL and task transformation strategies could handle multi-granularity reasoning tasks.
- We introduce two novel geospatial reasoning tasks, region reasoning and contour reasoning. We also provide the corresponding precisely annotated datasets to facilitate the advancement of remote sensing research.
- Holistic evaluations demonstrate that RemoteReasoner achieves superior generalization capabilities and efficiency in handling multi-granularity reasoning tasks through a single forward pass.

2. Related Work

2.1. Reasoning in Large Language Models

Recent efforts Jaech et al. (2024), Guo et al. (2025), Ren et al. (2024), Lai et al. (2024), Li et al. (2025) have shown that reasoning is central to aligning large language models (LLMs) with complex instructions. Models like OpenAI-o1 Jaech et al. (2024) and DeepSeek-R1 Guo et al. (2025) incorporate chain-of-thought(CoT) Wei et al. (2022) reasoning into their generation process, enabling flexible and interpretable multi-step inference. Both adopt reinforcement learning (RL) Kaelbling et al. (1996), Li (2017), Arulkumaran et al. (2017) to induce generalizable reasoning behaviors—OpenAI-o1 through RLHF and CoT monitoring, and DeepSeek-R1 via large-scale RL from scratch followed by multi-stage pretraining. These approaches exhibit strong reasoning capabilities but remain limited to natural language and vision tasks.

In remote sensing, models such as PixelLM Ren et al. (2024), LISA Lai et al. (2024), and SegEarth-R1 Li et al. (2025) extend reasoning to spatial domains. While effective for pixel- or region-level inference, they often support narrow task types and fixed granularity. Notably, SegEarth-R1 relies on supervised fine-tuning, making it less robust to distribution shifts and less adaptable in open-ended settings.

These limitations underscore the need for a more versatile geospatial framework. To this end, we propose RemoteReasoner, which supports unified and efficient multi-task, multi-granularity remote sensing understanding.

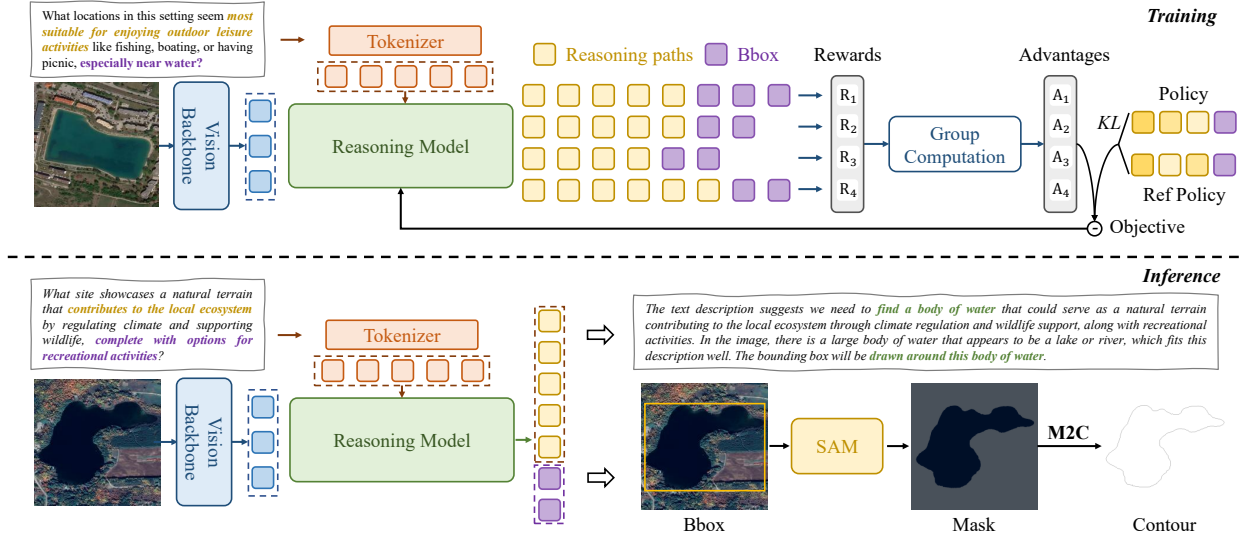


Figure 2: Overview of our RemoteReasoner. We utilize GPRO Shao et al. (2024) to explore model’s self-thinking capability. Then we design an inference workflow to perform multi-level reasoning tasks.

2.2. Remote Sensing Multi-modal Models

Recent remote sensing multimodal models Muhtar et al. (2024), Yao et al. (2025a), Zhan et al. (2024), Kuckreja et al. (2024), Yao et al. (2025b) demonstrate strong capabilities in handling diverse tasks across spatial granularities. Falcon Yao et al. (2025a) supports 14 vision-language tasks via multi-resolution encoding; GeoChat Kuckreja et al. (2024) and LHRS-Bot Muhtar et al. (2024) incorporate spatial prompts and geographic priors for improved region-level grounding; RemoteSAM Yao et al. (2025b) adopts a unified encoder for dense pixel-level segmentation; SkyEyeGPT Zhan et al. (2024) reformulates task input/output as natural language for broad task generalization. While effective in geospatial understanding, these models lack robust reasoning capabilities, limiting performance under ambiguous or compositional prompts.

While existing models demonstrate strong perception capabilities, they lack the reasoning ability to interpret complex prompts or adapt across granularities. RemoteReasoner addresses this gap by incorporating autonomous reasoning, enabling precise execution of complex natural language instructions and strong generalization across multi-granularity geospatial tasks.

3. RemoteReasoner

In this section, we introduce our method of building a workflow for multi-granularity geospatial reasoning tasks. The overall framework is represented in Fig. 2.

3.1. Data

The EarthReason Li et al. (2025) dataset is proposed alongside SegEarth-R1, containing 6 questions per sample with an average length of 20.86 words. It comprises 2,371 training, 1,135 validation, and 1,928 testing samples. However, this dataset is limited to pixel tasks. To address this, we generate detection and contour annotations through Mask2Bbox (M2B) Liu et al. (2024a) and Mask2Contour (M2C) Miao et al. (2025) strategies, respectively. Additionally, we design prompt templates combined

with original questions and generated bounding boxes to form training samples. The segmentation and contour annotations are exclusively reserved for downstream testing evaluation.

3.2. Reasoning Model

We utilize Qwen2.5-VL-7B-instruct Bai et al. (2025) as our reasoning model \mathcal{F}_θ . Despite Qwen2.5-VL’s superior performance in general-domain applications, direct adaptation to remote sensing imagery introduces domain knowledge discrepancy. Moreover, its reasoning capabilities require significant enhancement to address complex geospatial tasks. Therefore, we require fine-tuning it through reinforcement learning on remote sensing data.

3.3. Training

We utilize Group Relative Policy Optimization (GRPO) Shao et al. (2024) to train RemoteReasoner’s reasoning model. Unlike traditional reinforcement learning methods like PPO Schulman et al. (2017), GRPO directly compares groups of candidate outputs without an additional critic model. Given a query Q , GRPO samples N candidate outputs o_1, o_2, \dots, o_N from the policy π_θ . Then it computes each output o_i through a Reward function $R(Q, o_i)$. To determine the relative quality of the outputs, GRPO further normalizes the obtained rewards and subsequently derives the advantage:

$$A_i = \frac{r_i - \text{mean}\{r_1, r_2, \dots, r_N\}}{\text{std}\{r_1, r_2, \dots, r_N\}}, \quad (1)$$

where A_i denotes the advantage of o_i relative to other sampled outputs. GRPO aims to make the model generate outputs that obtain higher advantages, then utilize them to optimize the policy π_θ :

$$\begin{aligned} \mathcal{J}_{GRPO}(\theta) &= \mathbb{E}[\{o_i\}_{i=1}^N \sim \pi_{\theta_{old}}(q)] \\ &\frac{1}{N} \sum_{i=1}^N \{ \min[c_1 \cdot A_i, c_2 \cdot A_i] - \beta \text{D}_{KL}[\pi_\theta || \pi_{ref}] \}, \end{aligned} \quad (2)$$

where, c_1 and c_2 can be formulated as follows:

$$\begin{aligned} c_1 &= \frac{\pi_\theta(o_i|q)}{\pi_{\theta_{old}}(o_i|q)}, \\ c_2 &= \text{clip} \left(\frac{\pi_\theta(o_i|q)}{\pi_{\theta_{old}}(o_i|q)}, 1 + \epsilon, 1 - \epsilon \right). \end{aligned} \quad (3)$$

To adopt GRPO for our reasoning model, we design a composite reward function to optimize localization precision, object count accuracy, and output format. The total reward R combines 3 critical components:

- **Accuracy reward** measures bounding box alignment using Intersection-over-Union (IoU) with optimal Hungarian matching. For predicted boxes $B = \{b_k\}_{k=1}^K$ and ground truth $G = \{g_j\}_{j=1}^J$:

$$R_{IoU} = \frac{1}{|G|} \sum_{j=1}^{|G|} \max_k \left[\frac{|b_k \cap g_j|}{|b_k \cup g_j|} \right]. \quad (4)$$

- **Count reward** penalizes deviations in object quantity prediction using an exponential decay function:

$$R_{\text{count}} = \begin{cases} 1 & (J = 0) \wedge (K = 0) \\ 0 & (J = 0) \wedge (K > 0) , \\ \exp\left(-2 \cdot \frac{|K-J|}{J}\right) & J > 0 \end{cases} \quad (5)$$

where $J = |G|$ and $K = |B|$ denote ground-truth and predicted counts respectively. The exponential term $(-2 \cdot)$ creates a smooth penalty gradient that becomes stricter as relative count error increases.

- **Format reward** R_{format} checks whether RemoteReasoner’s outputs follow the specified format, returning 1 or 0 based on compliance. It is the JSON-style with reasoning paths in the `<think>...< /think>` tag and bboxes in the `<answer>[[x1,y1,x2,y2]...]< /answer>` tag.

Finally, the overall reward function is:

$$R = R_{\text{IoU}} + R_{\text{count}} + R_{\text{format}}. \quad (6)$$

3.4. Inference Workflow

After training, the reasoning model itself generates bounding boxes (bbox) indicating target regions. To further enhance the workflow and enable both pixel-level and object-level reasoning tasks, we need to leverage established tools. Specifically, we first input the bbox and its centroid coordinates to the SAM2 [Ravi et al. \(2024\)](#) to generate pixel-level masks. Subsequently, morphological operations are applied to analyze the mask images, extracting the outermost polygonal vertices to obtain target contours. The mathematical formulation of this process is presented as follows:

Given a remote sensing image $I \in \mathbb{R}^{H \times W \times 3}$ and a textual query Q , we define a multi-stage workflow for multi-task reasoning.

- **Geospatial Region Reasoning:** A vision-language model \mathcal{F}_θ processes the image-query pair (I, Q) to jointly produce:

$$(T, b) = \mathcal{F}_\theta(I, Q), \quad (7)$$

where T denotes the textual reasoning trace, and $b = [x_{\min}, y_{\min}, x_{\max}, y_{\max}]$ is the normalized bounding box of the target region.

- **Geospatial Pixel Reasoning:** The bounding box b and its center points v serve as prompts for the Segment Anything Model (SAM) \mathcal{S} . SAM generates a binary mask $M \in \{0, 1\}^{H \times W}$ isolating the target:

$$M = \mathcal{S}(I; b, v), \quad (8)$$

where $M_{(i,j)} = 1$ indicates pixel (i, j) belongs to the target.

- **Geospatial Contour Reasoning:** The target contour C is derived M via morphological boundary detection:

$$C = \Gamma(M) = \{(x_k, y_k)\}_{k=1}^K, \quad (9)$$

where $\Gamma(\cdot)$ extracts the polygonal vertices $\{(x_k, y_k)\}$ of the mask’s external boundary.

Table 1: Geospatial Pixel Reasoning Results on EarthReason. It is worth noting that RemoteReasoner was not trained directly utilizing its segmentation labels.

Method	<i>cIoU</i>		<i>gIoU</i>	
	Val	Test	Val	Test
<i>SFT Methods</i>				
LISA Lai et al. (2024)	57.39	59.10	61.04	60.88
PixelLM Ren et al. (2024)	57.79	59.22	57.94	60.01
PSALM Zhang et al. (2024)	62.03	64.61	66.61	68.30
SegEarth-R1 Li et al. (2025)	64.13	68.25	68.60	70.75
<i>RL Method</i>				
RemoteReasoner	67.80	69.13	69.02	70.96

Table 2: Geospatial Region Reasoning Results.

Method	<i>Acc@0.5</i>		<i>gIoU</i>	
	Val	Test	Val	Test
DeepSeek-VL2-tiny Guo et al. (2025)	12.08	12.67	17.51	18.62
GeoChat Kuckreja et al. (2024)	10.10	8.89	12.57	11.44
Qwen2.5-VL-7B Bai et al. (2025)	41.21	45.82	38.77	41.80
RemoteReasoner	66.51	68.11	67.04	69.29

4. Experiments

4.1. Dataset and Metrics

Dataset. We evaluate on the validation and test sets of EarthReason Li et al. (2025). Pixel-level tasks directly utilize the original annotations, while region-level and object-level tasks are transformed using M2B Liu et al. (2024a) and M2C Miao et al. (2025) annotation formats based on the original labels, respectively. Additionally, we employ the RSVG Zhan et al. (2023) test set for Visual Grounding evaluation and the RRSISD Liu et al. (2024b) test set for Referring Expression Segmentation tasks, with their training sets explicitly excluded from model training. For unseen category evaluation, we manually selected 100 images covering 10 distinct unseen categories from the RemoteSAM-270K Yao et al. (2025b) dataset.

Metrics. Following previous works Yao et al. (2025b), Li et al. (2025), we adopt *gIoU*, *cIoU*, and *Acc@0.5* as region- and pixel-level evaluation metrics. For contour reasoning, we employ F1 score with 1-pixel and 3-pixel dilated kernel ($F1@1$ & $F1@3$) as evaluation metrics, and incorporate two geometric error measures: Average Symmetric Distance (*ASD*) and Hausdorff Distance (*HD*).

4.2. Implementations Details

We employ GRPO Shao et al. (2024) to fine-tune the Qwen2.5-VL-7B-Instruct Bai et al. (2025) model using LoRA Hu et al. (2022) (rank=8, alpha=16, targeting all linear layers). Training is conducted for 24 epochs on $8 \times$ NVIDIA L20 GPUs with a global batch size of 512 (achieved via per-device batch size 8 and gradient accumulation steps 8), using the AdamW Loshchilov and Hutter (2017) optimizer with a learning rate of 1e-6, bf16 precision, and DeepSpeed Rasley et al. (2020) Zero3 for memory efficiency.

Table 3: Geospatial Contour Reasoning Results on EarthReason.

Method	F1@1↑		F1@3↑		ASD↓		HD↓	
	Val	Test	Val	Test	Val	Test	Val	Test
EPOC Chen et al. (2024a)	0.10	0.10	0.19	0.20	60.07	64.38	243.98	255.81
RemoteReasoner	0.46	0.44	0.55	0.58	41.50	45.20	160.56	165.11

4.3. Main Results

4.3.1. Geospatial Region Reasoning

This section validates RemoteReasoner’s performance on region-level reasoning tasks, with results presented in Tab. 2. Compared to the remote sensing multi-modal foundation model GeoChat [Kuckreja et al. \(2024\)](#), RemoteReasoner demonstrates at least a 56.41% improvement. This significant gain stems from GeoChat’s weak reasoning capabilities, which fail to interpret ambiguous queries. Similarly, RemoteReasoner achieves over 22.39% improvement against general-purpose MLLMs, *e.g.*, Qwen-2.5VL-7B [Bai et al. \(2025\)](#) and DeepSeek-VL2-tiny (3B) [Guo et al. \(2025\)](#). Although these MLLMs possess basic reasoning abilities, their insufficient domain-specific knowledge in remote sensing leads to suboptimal performance on geospatial region-level reasoning tasks.

4.3.2. Geospatial Pixel Reasoning

We evaluate RemoteReasoner’s performance on pixel-level reasoning tasks using the EarthReason dataset. We compare against state-of-the-art general-domain methods (LISA [Lai et al. \(2024\)](#), PixelLM [Ren et al. \(2024\)](#), PSALM [Zhang et al. \(2024\)](#)) and the remote sensing-domain SegEarth-R1 [Li et al. \(2025\)](#), with results summarized in Tab. 1. Experimental results demonstrate that despite not directly utilizing pixel-level labels during training, our approach remarkably surpasses SFT-based methods that leverage both pixel annotations and reasoning trajectories. For instance, RemoteReasoner achieves 10.41% higher *cIoU* than LISA on the validation set. Compared to the best-performing SegEarth-R1, we observe a 3.67% improvement. The primary reason lies in the superior robustness of reinforcement learning (RL) frameworks compared to supervised fine-tuning (SFT) paradigms. Even without direct exposure to pixel-level annotations, our model effectively utilizes bounding boxes to prompt the Segment Anything Model (SAM), achieving precise segmentation results through this indirect yet efficient interaction mechanism.

4.3.3. Geospatial Contour Reasoning

This section validates the contour extraction performance of RemoteReasoner. We select EPOC [Chen et al. \(2024a\)](#) as a comparative baseline. Since EPOC lacks reasoning capabilities, we crop the bounding boxes (bbox) generated by RemoteReasoner and input them into EPOC to obtain contours, as shown in Fig. 3. Since EPOC is class-agnostic, it extracts contours for all objects within the region (*e.g.*, first and third rows). In contrast, RemoteReasoner’s contours are derived from segmentation masks, resulting in tighter alignment with target boundaries. Furthermore, under low-resolution conditions (second row), EPOC produces blurry or disconnected contours, whereas our method maintains sharp and closed boundaries.

Quantitative results (as shown in Tab. 3) demonstrate that RemoteReasoner surpasses EPOC by at least 0.34 in both F1 scores, with significantly lower distance errors compared to EPOC. This

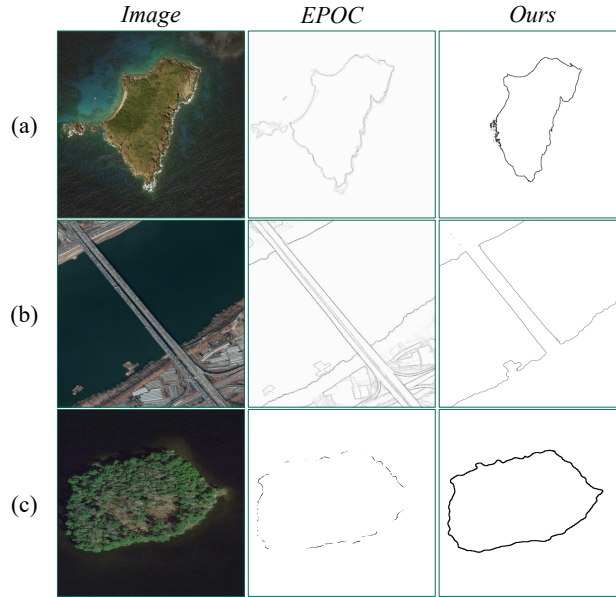


Figure 3: Geospatial Contour Reasoning Results. We select EPOC [Chen et al. \(2024a\)](#) for comparison.

performance gap can be attributed to EPOC’s tendency to extract extraneous contours and its failure to handle indistinct target boundaries effectively.

4.4. Further Analysis

After reinforcement learning training, can the reasoning model maintain the original capabilities of the MLLM? To explore this, we evaluate RemoteReasoner’s extrinsic capabilities, including its ability to handle unseen task types and recognize out-of-distribution categories.

4.4.1. Can RemoteReasoner Do Other Tasks?

We evaluate RemoteReasoner on Visual Grounding and Referring Expression Segmentation tasks, with results summarized in Tab. 4. Comparative experiments are conducted against state-of-the-art LLM-based approaches, including general-domain methods (MiniGPT-V2 [Zhu et al. \(2023\)](#), LISA [Lai et al. \(2024\)](#), PixelLM [Ren et al. \(2024\)](#)) and remote sensing-specific frameworks (Falcon [Yao et al. \(2025a\)](#), LHRS-Bot [Muhtar et al. \(2024\)](#), GeoGround [Zhou et al. \(2024\)](#)). Notably, all remote sensing methods were trained on task-specific data, while RemoteReasoner’s zero-shot performance achieves 80% of their supervised results. Under identical zero-shot settings, our framework achieves gains of 4.12% on Visual Grounding and 19.32% on Referring Expression Segmentation tasks.

Furthermore, as the workflow’s core component is a multi-modal large language model, we verify preservation of its inherent capabilities through multi-turn dialogue evaluation (Fig. 4). The model first performs image captioning, then accurately answers content-based questions about the image. Additional results are provided in the supplementary material. These results demonstrate our framework’s strong generalization capabilities with RL.

Table 4: Performance on unseen tasks. VG and RES are Visual Grounding and Referring Expression Segmentation.

Task	Method	Acc@0.5	<i>gIoU</i>
VG	<i>Trained</i>		
	MGVLF Zhan et al. (2023)	76.78	68.04
	Falcon Yao et al. (2025a)	56.87	-
	SkyEyeGPT Zhan et al. (2024)	70.50	-
	LHRS-Bot Muhtar et al. (2024)	73.45	-
	<i>Zero-shot</i>		
	MiniGPT-V2 Zhu et al. (2023)	46.64	-
Qwen-VL-Chat Hui et al. (2024)	44.76	-	
	RemoteReasoner	50.76	49.85
Task	Method	<i>cIoU</i>	<i>gIoU</i>
RES	<i>Trained</i>		
	GeoGround Zhou et al. (2024)	-	60.50
	SegEarth-R1 Li et al. (2025)	67.56	66.40
	<i>Zero-shot</i>		
	LISA Lai et al. (2024)	-	26.78
	PixelLM Ren et al. (2024)	-	31.65
	RemoteReasoner	54.29	50.97

Table 5: Out-of-distribution category recognition performance. We manually select 10 novel classes that are absent in EarthReason.

Category	Car	Ship	Field	Apron	Grass
<i>gIoU</i>	21.56	50.03	36.72	54.09	38.27
Category	Trucks	Hangar	Parking	Roof	Warehouses
<i>gIoU</i>	25.58	58.34	30.52	52.85	41.00

4.4.2. Can RemoteReasoner Recognize Other Category?

Given that the EarthReason Li et al. (2025) dataset contains only 28 categories, which is significantly insufficient to cover common remote sensing targets. Therefore, we further investigate RemoteReasoner’s recognition capability for unseen categories. We manually select 100 images spanning 10 novel categories from RemoteSAM-270K Yao et al. (2025b) that are absent in EarthReason for evaluation. As represented in Tab. 5, RemoteReasoner demonstrates robust recognition of out-of-distribution categories with consistent accuracy. It demonstrates that our RL strategy avoids overfitting to category distributions in the training data. However, the model still exhibits insufficient capabilities in detecting small objects (e.g., , cars), indicating a direction for future research.

4.4.3. Qualitative Analysis

The qualitative results of the three supported tasks in our workflow are presented in Fig. 5. In the first sample row, the user seeks a venue for group sports, while a baseball field nearly blends into the background in the image. RemoteReasoner correctly reasons and locates the target, simultaneously yielding its segmentation mask and contour. The second row shows a relatively blurred image of

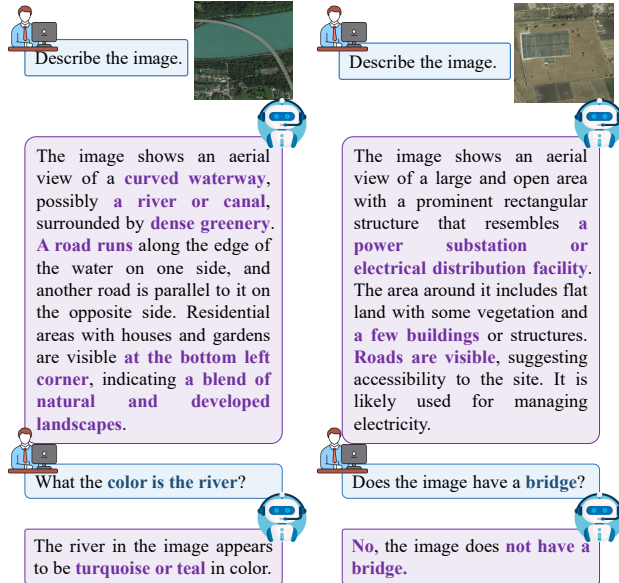


Figure 4: Quantitative results of other tasks (Image Captioning & VQA).

Table 6: Ablation on different pixel-level output formats. Text2Mask denotes LLM-generated textual polygon.

Output Format	Training Method	$cIoU$	$gIoU$
Text2Mask	SFT	22.01	22.97
	RL	18.74	19.21
Bbox2Mask	SFT	60.25	62.19
	RL	69.13	70.96

a medical helipad. Based on its function of providing emergency rescue services, RemoteReasoner accurately locates and segments the target area along with its contour. These visualizations indicate that our method can adapt to challenging reasoning tasks.

4.5. Ablation Studies

4.5.1. Different Pixel-level Output Formats

Recently, RemoteSAM Yao et al. (2025b) validates that segmentation, as a fundamental visual output unit, enables bottom-up transformation to other vision tasks. Therefore, if LLMs could directly generate masks in textual representations, the architectural design holds promise for greater unification. To explore this hypothesis, we conducted experiments using such formulations, as summarized in Tab. 6. However, textual outputs prove ill-suited for this predictive task, with both SFT and RL strategies exhibiting significant performance degradation compared to visual-based approaches. In contrast, directly outputting bounding boxes and then generating masks through SAM significantly outperforms textual mask representations (22.01 vs. 60.25). When incorporating RL strategies, the accuracy further improves from 60.25 to 69.13. Based on these findings, we adopt the Mask2Contour approach in our workflow design.

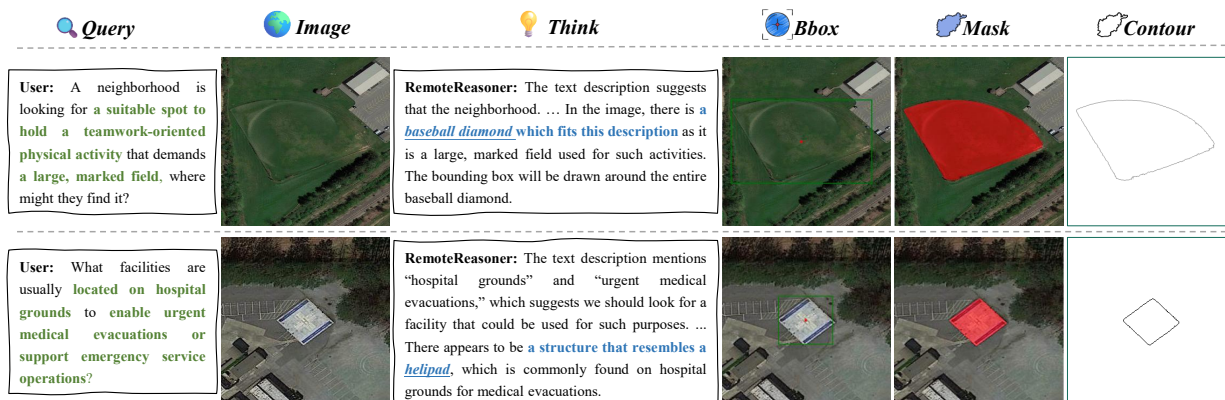


Figure 5: Quantitative Results. Given an image and its corresponding implicit query, RemoteReasoner autonomously identifies the user-intended target category through reasoning and accurately executes visual-centric tasks across three granularities.

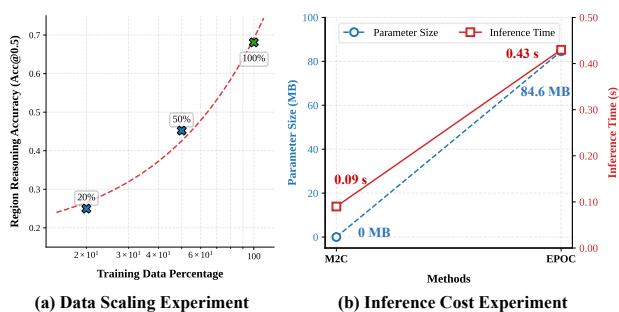


Figure 6: (a) Data scaling experiment. We observed that the model performance increases as the data scales exponentially. (b) Inference cost experiment. Mask2Contour method achieved significantly faster inference speed.

4.5.2. Data Scaling Experiment

To validate data impact on model performance, we evaluate it by training with 20%, 50% and 100% subsets of the full training data. As illustrated in Fig. 6 (a), the results demonstrate that model performance improves with increasing data scale. The full dataset (100%) achieves the best performance, indicating the current data scale contains no redundancy. These findings suggest that geospatial reasoning tasks retain untapped potential that can be unlocked through larger data scales.

4.5.3. Inference Cost Ablation

We further evaluate inference speed across different contour extraction strategies, as shown in Fig. 6 (b). The Mask2Contour approach directly applies morphological operations without introducing additional parameters, achieving significantly faster processing speed (0.09s per image). In contrast, EPOC, as a deep learning model with 84.6MB parameters, demonstrates inferior inference speed (0.43s per image). This comparison highlights the efficiency advantages of our proposed workflow.

5. Conclusion & Limitations

Conclusion. We present RemoteReasoner, a novel workflow advancing autonomous geospatial reasoning. Overcoming limitations of SFT-based approaches, it leverages RL strategy to cultivate robust reasoning capabilities while preserving MLLM generalization. Its core innovation is a unified inference pipeline enabling efficient multi-granularity task transformation (pixel-, region-, and object-level) from a single MLLM output, eliminating redundant per-task decoders. RemoteReasoner achieves SOTA results, including > 15% and 30% accuracy gains in region- and object-level reasoning, and demonstrates superior generalization across diverse, complex queries. It provides a flexible foundation for downstream geospatial intelligence requiring nuanced intent interpretation and multi-format outputs.

Limitations. Despite the advantages, several limitations exist for future improvement. First, model performance remains limited by current reasoning dataset scale. Progress will require more comprehensive datasets. Second, the performance on small objects needs enhancement via specialized data and architectural refinements. Additionally, exploring more tasks could advance unified geospatial reasoning.

References

- Adekanmi Adeyinka Adegun, Serestina Viriri, and Jules-Raymond Tapamo. Review of deep learning methods for remote sensing satellite images classification: experimental survey and comparative analysis. *Journal of Big Data*, 10(1):93, 2023.
- Kai Arulkumaran, Marc Peter Deisenroth, Miles Brundage, and Anil Anthony Bharath. Deep reinforcement learning: A brief survey. *IEEE SPM*, 34(6):26–38, 2017.
- Shuai Bai, Keqin Chen, Xuejing Liu, Jialin Wang, Wenbin Ge, Sibao Song, Kai Dang, Peng Wang, Shijie Wang, Jun Tang, et al. Qwen2. 5-vl technical report. *arXiv preprint arXiv:2502.13923*, 2025.
- Kilian Carolan, Laura Fennelly, and Alan F Smeaton. A review of multi-modal large language and vision models. *arXiv preprint arXiv:2404.01322*, 2024.
- Delong Chen, Samuel Cahyawijaya, Jianfeng Liu, Baoyuan Wang, and Pascale Fung. Subobject-level image tokenization. *arXiv preprint arXiv:2402.14327*, 2024a.
- Yi-Chia Chen, Wei-Hua Li, Cheng Sun, Yu-Chiang Frank Wang, and Chu-Song Chen. Sam4mllm: Enhance multi-modal large language model for referring expression segmentation. In *ECCV*, pages 323–340. Springer, 2024b.
- Daya Guo, Dejian Yang, Haowei Zhang, Junxiao Song, Ruoyu Zhang, Runxin Xu, Qihao Zhu, Shirong Ma, Peiyi Wang, Xiao Bi, et al. Deepseek-r1: Incentivizing reasoning capability in llms via reinforcement learning. *arXiv preprint arXiv:2501.12948*, 2025.
- Edward J Hu, Yelong Shen, Phillip Wallis, Zeyuan Allen-Zhu, Yuanzhi Li, Shean Wang, Lu Wang, Weizhu Chen, et al. Lora: Low-rank adaptation of large language models. *ICLR*, 1(2):3, 2022.
- Binyuan Hui, Jian Yang, Zeyu Cui, Jiayi Yang, Dayiheng Liu, Lei Zhang, Tianyu Liu, Jiajun Zhang, Bowen Yu, Keming Lu, et al. Qwen2. 5-coder technical report. *arXiv preprint arXiv:2409.12186*, 2024.
- Aaron Jaech, Adam Kalai, Adam Lerer, Adam Richardson, Ahmed El-Kishky, Aiden Low, Alec Hel- yar, Aleksander Madry, Alex Beutel, Alex Carney, et al. Openai o1 system card. *arXiv preprint arXiv:2412.16720*, 2024.
- Leslie Pack Kaelbling, Michael L Littman, and Andrew W Moore. Reinforcement learning: A survey. *Journal of artificial intelligence research*, 4:237–285, 1996.
- Kartik Kuckreja, Muhammad Sohail Danish, Muzammal Naseer, Abhijit Das, Salman Khan, and Fahad Shahbaz Khan. Geochat: Grounded large vision-language model for remote sensing. In *CVPR*, pages 27831–27840, 2024.
- Xin Lai, Zhuotao Tian, Yukang Chen, Yanwei Li, Yuhui Yuan, Shu Liu, and Jiaya Jia. Lisa: Reasoning segmentation via large language model. In *CVPR*, pages 9579–9589, 2024.
- Kaiyu Li, Zepeng Xin, Li Pang, Chao Pang, Yupeng Deng, Jing Yao, Guisong Xia, Deyu Meng, Zhi Wang, and Xiangyong Cao. Segearth-r1: Geospatial pixel reasoning via large language model. *arXiv preprint arXiv:2504.09644*, 2025.
- Yuxi Li. Deep reinforcement learning: An overview. *arXiv preprint arXiv:1701.07274*, 2017.

- Fan Liu, Delong Chen, Zhangqingyun Guan, Xiacong Zhou, Jiale Zhu, Qiaolin Ye, Liyong Fu, and Jun Zhou. Remoteclip: A vision language foundation model for remote sensing. *IEEE TGRS*, 62: 1–16, 2024a.
- Fan Liu, Liang Yao, Chuanyi Zhang, Ting Wu, Xinlei Zhang, Xiruo Jiang, and Jun Zhou. Boost uav-based object detection via scale-invariant feature disentanglement and adversarial learning. *IEEE TGRS*, 2025a.
- Sihan Liu, Yiwei Ma, Xiaoqing Zhang, Haowei Wang, Jiayi Ji, Xiaoshuai Sun, and Rongrong Ji. Rotated multi-scale interaction network for referring remote sensing image segmentation. In *CVPR*, pages 26658–26668, 2024b.
- Yuqi Liu, Bohao Peng, Zhisheng Zhong, Zihao Yue, Fanbin Lu, Bei Yu, and Jiaya Jia. Seg-zero: Reasoning-chain guided segmentation via cognitive reinforcement. *arXiv preprint arXiv:2503.06520*, 2025b.
- Ilya Loshchilov and Frank Hutter. Decoupled weight decay regularization. *arXiv preprint arXiv:1711.05101*, 2017.
- Shiyu Miao, Delong Chen, Fan Liu, Chuanyi Zhang, Yanhui Gu, Shengjie Guo, and Jun Zhou. Prompting directsam for semantic contour extraction in remote sensing images. In *ICASSP 2025*, pages 1–5. IEEE, 2025.
- Dilxat Muhtar, Zhenshi Li, Feng Gu, Xueliang Zhang, and Pengfeng Xiao. Lhrs-bot: Empowering remote sensing with vgi-enhanced large multimodal language model. In *ECCV*, pages 440–457. Springer, 2024.
- Jeff Rasley, Samyam Rajbhandari, Olatunji Ruwase, and Yuxiong He. Deepspeed: System optimizations enable training deep learning models with over 100 billion parameters. In *Proceedings of the 26th ACM SIGKDD international conference on knowledge discovery & data mining*, pages 3505–3506, 2020.
- Nikhila Ravi, Valentin Gabeur, Yuan-Ting Hu, Ronghang Hu, Chaitanya Ryali, Tengyu Ma, Haitham Khedr, Roman Rädle, Chloe Rolland, Laura Gustafson, et al. Sam 2: Segment anything in images and videos. *arXiv preprint arXiv:2408.00714*, 2024.
- Zhongwei Ren, Zhicheng Huang, Yunchao Wei, Yao Zhao, Dongmei Fu, Jiashi Feng, and Xiaojie Jin. Pixellm: Pixel reasoning with large multimodal model. In *CVPR*, pages 26374–26383, 2024.
- John Schulman, Filip Wolski, Prafulla Dhariwal, Alec Radford, and Oleg Klimov. Proximal policy optimization algorithms. *arXiv preprint arXiv:1707.06347*, 2017.
- Zhihong Shao, Peiyi Wang, Qihao Zhu, Runxin Xu, Junxiao Song, Xiao Bi, Haowei Zhang, Mingchuan Zhang, YK Li, Yang Wu, et al. Deepseekmath: Pushing the limits of mathematical reasoning in open language models. *arXiv preprint arXiv:2402.03300*, 2024.
- Haozhan Shen, Peng Liu, Jingcheng Li, Chunxin Fang, Yibo Ma, Jiajia Liao, Qiaoli Shen, Zilun Zhang, Kangjia Zhao, Qianqian Zhang, et al. Vlm-r1: A stable and generalizable r1-style large vision-language model. *arXiv preprint arXiv:2504.07615*, 2025.
- Junjue Wang, Zhuo Zheng, Zihang Chen, Ailong Ma, and Yanfei Zhong. Earthvqa: Towards queryable earth via relational reasoning-based remote sensing visual question answering. In *AAAI*, volume 38, pages 5481–5489, 2024.

- Jason Wei, Xuezhi Wang, Dale Schuurmans, Maarten Bosma, Fei Xia, Ed Chi, Quoc V Le, Denny Zhou, et al. Chain-of-thought prompting elicits reasoning in large language models. *NeurIPS*, 35: 24824–24837, 2022.
- Fengli Xu, Qianyu Hao, Zefang Zong, Jingwei Wang, Yunke Zhang, Jingyi Wang, Xiaochong Lan, Jiahui Gong, Tianjian Ouyang, Fanjin Meng, et al. Towards large reasoning models: A survey of reinforced reasoning with large language models. *arXiv preprint arXiv:2501.09686*, 2025.
- Kelu Yao, Nuo Xu, Rong Yang, Yingying Xu, Zhuoyan Gao, Titinunt Kitrungrotsakul, Yi Ren, Pu Zhang, Jin Wang, Ning Wei, et al. Falcon: A remote sensing vision-language foundation model. *arXiv preprint arXiv:2503.11070*, 2025a.
- Liang Yao, Fan Liu, Delong Chen, Chuanyi Zhang, Yijun Wang, Ziyun Chen, Wei Xu, Shimin Di, and Yuhui Zheng. Remotesam: Towards segment anything for earth observation. *arXiv preprint arXiv:2505.18022*, 2025b.
- Yang Zhan, Zhitong Xiong, and Yuan Yuan. Rsvg: Exploring data and models for visual grounding on remote sensing data. *IEEE TGRS*, 61:1–13, 2023.
- Yang Zhan, Zhitong Xiong, and Yuan Yuan. Skyeyegpt: Unifying remote sensing vision-language tasks via instruction tuning with large language model, 2024. URL <https://arxiv.org/abs/2401.09712>.
- Zheng Zhang, Yeyao Ma, Enming Zhang, and Xiang Bai. Psalm: Pixelwise segmentation with large multi-modal model. In *ECCV*, pages 74–91. Springer, 2024.
- Zixiao Zhang, Licheng Jiao, Lingling Li, Xu Liu, Puhua Chen, Fang Liu, Yuxuan Li, and Zhicheng Guo. A spatial hierarchical reasoning network for remote sensing visual question answering. *IEEE TGRS*, 61:1–15, 2023.
- Tianjie Zhao, Sheng Wang, Chaojun Ouyang, Min Chen, Chenying Liu, Jin Zhang, Long Yu, Fei Wang, Yong Xie, Jun Li, et al. Artificial intelligence for geoscience: Progress, challenges, and perspectives. *The Innovation*, 5(5), 2024.
- Yue Zhou, Mengcheng Lan, Xiang Li, Yiping Ke, Xue Jiang, Litong Feng, and Wayne Zhang. Geoground: A unified large vision-language model. for remote sensing visual grounding. *arXiv preprint arXiv:2411.11904*, 2024.
- Deyao Zhu, Jun Chen, Xiaoqian Shen, Xiang Li, and Mohamed Elhoseiny. Minigpt-4: Enhancing vision-language understanding with advanced large language models. *arXiv preprint arXiv:2304.10592*, 2023.
- Zhengxia Zou, Keyan Chen, Zhenwei Shi, Yuhong Guo, and Jieping Ye. Object detection in 20 years: A survey. *Proceedings of the IEEE*, 111(3):257–276, 2023.

Appendix of RemoteReasoner

A. More Implementation Details

The training pipeline leverages MS-SWIFT framework with Group Relative Preference Optimization (GRPO). Experiments use $8 \times$ NVIDIA L20 GPUs with DeepSpeed Zero-3 for memory optimization. We initialize weights from Qwen2.5-VL-7B-Instruct and apply LoRA adaptation (rank 8, $\alpha = 16$) to all linear layers. The training configuration employs a global batch size of 512 (8 per-device batches \times 8 gradient accumulation steps \times 8 GPUs), bfloat16 precision, and flash attention for computational efficiency. We train for 24 epochs with a learning rate of 1×10^{-6} , linear warmup (5% of steps), and gradient checkpointing. Input sequences are capped at 4096 tokens with image resolution limited to 802816 pixels. The optimizer uses AdamW with weight decay disabled. For RLHF alignment, we utilize a temperature of 0.9 during generation.

B. More Experiments

B.1 Balance Factors Sensitive Analysis

Table 7: Balance Factors Sensitive Analysis of Accuracy Rewards.

<i>gIoU</i>	0.3	0.5	0.7	1
0.3	47.24	46.73	46.22	48.01
0.5	45.21	46.85	48.03	49.26
0.7	47.07	46.90	49.88	49.05
1	47.78	49.67	48.95	50.11

Before training, to obtain an optimal set of balance factors for the reward function, we sampled a small portion of the dataset and trained the model using different weighting schemes for the accuracy rewards. Tab. 7 presents a sensitivity analysis of the reward function balance factors, each ranging from 0.3 to 1.0. The values represent model performance under each configuration on the validation set. Among all tested combinations, the setting where both balance factors are set to 1.0 achieves the best performance, reaching 50.11%. Compared to lower-weighted settings, the (1.0, 1.0) configuration provides stronger and more consistent supervision, leading to more effective optimization. Therefore, we adopt this configuration in our final model training.

B.2 Point Prompt Effectiveness Ablations

Table 8: Effectiveness of different prompts to SAM. We directly calculate bbox’s center point without letting LLM output additional points.

Bbox	Point	<i>cIoU</i>	<i>gIoU</i>
✓		43.09	42.41
✓	✓	69.13	70.96

To evaluate the effectiveness of different prompt types in guiding the SAM model, we conducted a controlled experiment using bounding box (bbox) and center point prompts. Specifically, we compare two settings: using only bbox prompts, and using both bbox and point prompts, where the point is

simply computed as the center of the bbox—without relying on additional points generated by the LLM. As shown in the Tab. 8, using only the bbox yields moderate performance with 43.09 $cIoU$ and 42.41 $gIoU$. However, when the center point is additionally provided as a prompt, performance improves significantly to 69.13 $cIoU$ and 70.96 $gIoU$. This substantial gain highlights the complementary role of point prompts in guiding the segmentation process. The result suggests that even simple, derived point inputs (like bbox centers) can substantially enhance SAM’s segmentation accuracy when used in conjunction with bounding boxes.

C. More Qualitative Results

In this section, we present additional visualizations for multi-granularity reasoning tasks. Results for region-level and pixel-level reasoning are illustrated in Fig. 7, while contour reasoning outcomes appear in Fig. 8. Results incorporating the reasoning process are depicted in Fig. 9 and 10. Additionally, we provide image-level task results—including Visual Question Answering (VQA) and image captioning—as summarized in Fig. 11 and 12.

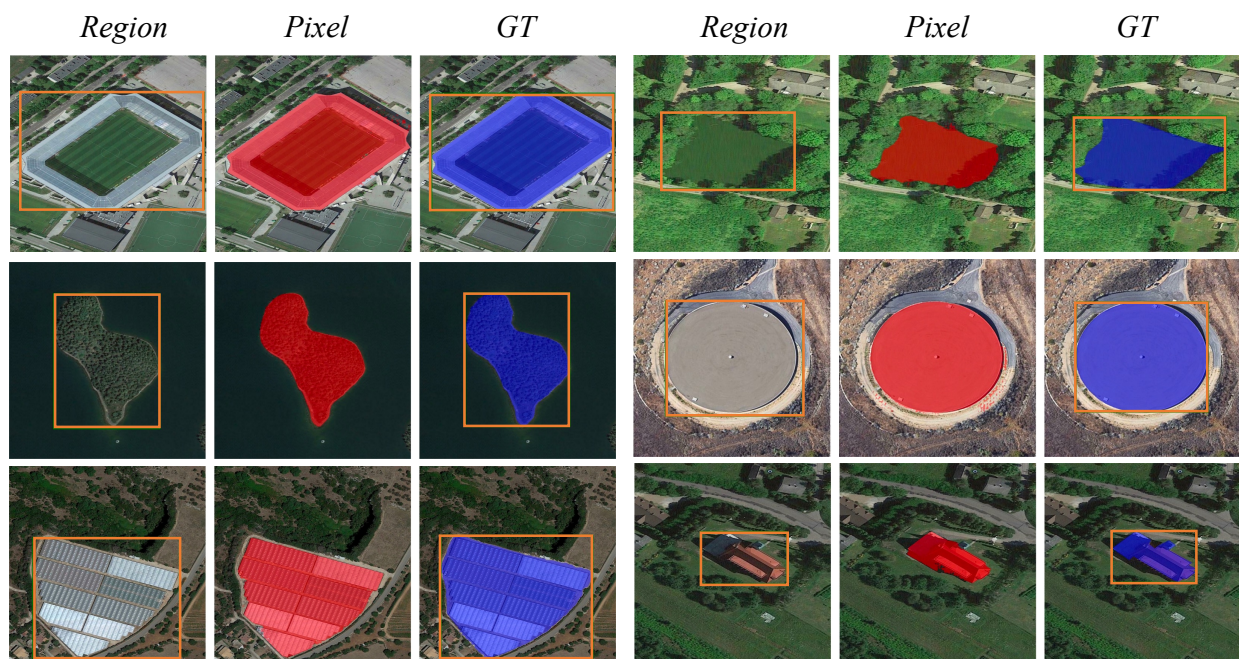


Figure 7: Region- (detection) and Pixel-level (segmentation) Results.

D Failure Case Analysis

Fig. 13 presents several illustrative failure cases of RemoteReasoner. First row: The query requests an entity that circumvents the urban core (expected: an overpass). However, the model incorrectly classifies the entire intersection as fulfilling this condition, consequently outputting its complete structure. Second row: The query requires locating the grandstand. While the model outputs the entire baseball stadium, the reasoning process leading to this output is logically sound. It is noteworthy that the ground truth annotation for this sample is also incorrect, as it fails to label the grandstand location. Third row: The model mistakenly incorporates the shadow region as part of the target object. These failure cases highlight significant areas for improvement in our method.



Figure 8: Object-level (contour extraction) Results.

E. Prompts Setting

We present the prompt templates designed during dataset construction in Tab. 9.

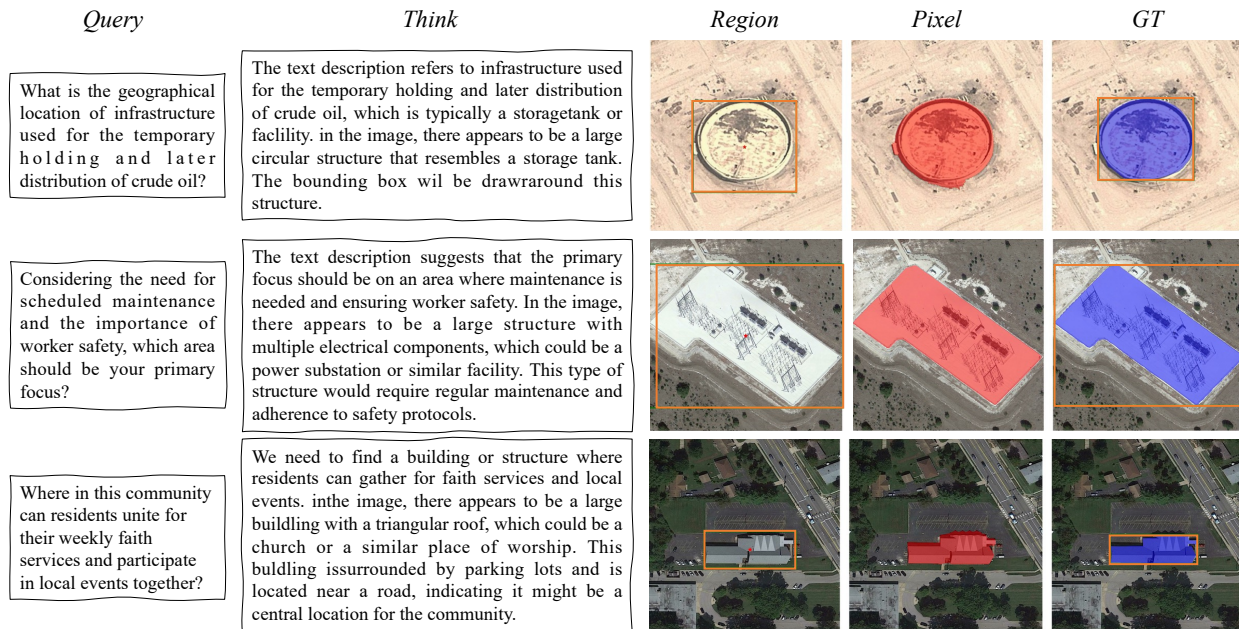


Figure 9: More Geospatial Reasoning Results (part 1).

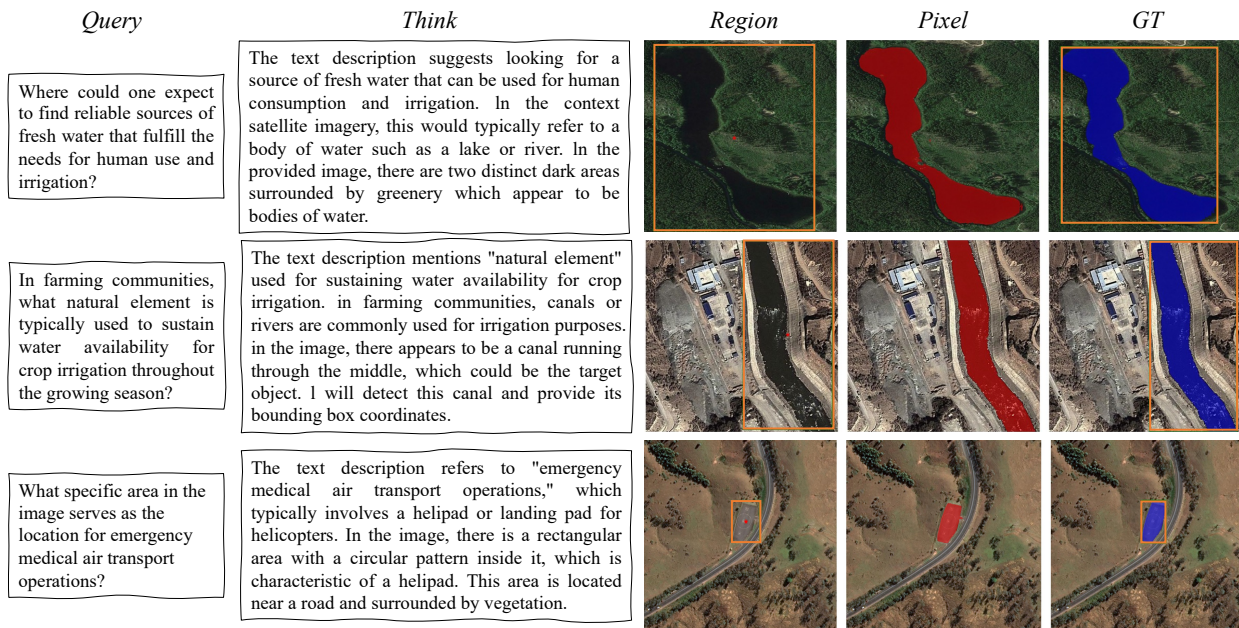


Figure 10: More Geospatial Reasoning Results (part 2).



Q: How many ships in the image?

Think: The image provided is an aerial view of a river with some infrastructure around it. There are visible watercraft on the river, which appear to be ships or barges. To determine the number of ships, I'll count each distinct vessel.

A: 4



Q: The venue in the image can be used for what sports?

Think: The image shows an aerial view of a large stadium with a green field that appears to be designed for soccer (football). The presence of goalposts at each end of the field further supports this conclusion. Stadiums like this are typically used for soccer matches.

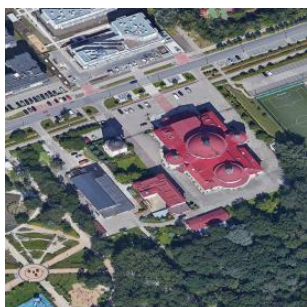
A: Soccer (football)



Q: The venue in the image can be used for what sports?

Think: The image shows a large area with a runway and surrounding buildings, which indicates that it is located near an airport. The presence of a runway suggests that this area is not entirely rural but rather part of an urban environment where there is infrastructure for air travel. They are characteristic of urban settings.

A: Urban.



Q: How many red roof buildings in the image?

Think: To determine how many red-roofed buildings are in the image, I'll carefully examine the structure in the center of the image. It appears to be a complex with multiple interconnected sections, all featuring red roofs. I'll count each distinct section that has a red roof.

A: Three.



Q: What the shape is the island?

Think: The image shows an island that appears to be crescent-shaped or moon-like. This can be inferred from the curved outline of the landmass and the way it wraps around itself, creating a shape that resembles a crescent.

A: The island is shaped like a crescent or moon.

Figure 11: More Qualitative Results of Visual Question Answering.



This image depicts an aerial view of a developed area with a prominent waterway (likely a river or canal) running through it. There are multiple roads and bridges crossing the waterway, suggesting a well-connected transportation network. The surrounding areas include industrial buildings, construction sites, and open land plots that seem to be undergoing development. Green spaces and what appears to be a park area are located near the water's edge. The presence of barges indicates potential use for transportation or as part of a port system. The area combines urban development with industrial activities.



The image shows an aerial view of Banc of California Stadium, a large soccer stadium located in Los Angeles, California. It features a modern design with a curved roof and multiple tiers of seating. The field is marked for soccer, and there's visible construction or development activity around the stadium. The name "Banc of California" is clearly visible on the stadium's exterior.



The image depicts an airport runway with a grassy area and white marking lines, situated within an urban environment. Surrounding the runway are various buildings and structures, and there appears to be solar panel installations nearby, indicating a focus on renewable energy. The area is densely built-up, suggesting the airport is located close to a city or town.



The image shows an aerial view of a complex with a prominent building featuring red domed roofs, likely a religious or educational institution. The surrounding area includes parking lots, green spaces, and nearby roads, indicating it's situated in a developed area. The design and layout suggest it could be a monastery, school, or similar institution.



The image shows a crescent-shaped island with a rugged coastline and green vegetation at its center. The surrounding water is a vibrant turquoise color, transitioning to deeper blue further away from the island. This suggests a shallow coastal area near the island and deeper ocean waters beyond.

Figure 12: More Qualitative Results of Image Captioning.

<i>Query</i>	<i>Think</i>	<i>Region</i>	<i>Pixel</i>	<i>GT</i>
<p>If your goal is to design a transport pathway that circumvents the urban core, which infrastructure elements would be essential, and why?</p>	<p>In the context of the image, highways or roads are essential infrastructure elements for such a purpose. The image shows a highway intersection, which is a critical part of the transportation network. The bounding box coordinates will be determined by identifying the area encompassing this highway intersection.</p>			
<p>Considering the image, where do you think is the best spot for a local sports event, allowing spectators to watch with ease?</p>	<p>The text description suggests looking for a location that would allow spectators to watch a local sports event easily. In the context of the image, this would likely refer to a baseball field or a similar sports venue where spectators can sit and watch the game from the stands. The image shows a baseball field with a dirt infield and grass outfield, surrounded by what appears to be spectator seating areas</p>			
<p>Can you identify the type of infrastructure employed to manage substantial storage of liquids or gases, promoting the continuity of industrial activities?</p>	<p>The text description refers to infrastructure used for managing the storage of liquids or gases, which is typically associated with industrial facilities such as oil tanks, water reservoirs, or chemical storage tanks. In the image, there appears to be a large circular structure that resembles a storage tank, which could be used for storing liquids or gases.</p>			

Figure 13: Failure Case Qualitative Results.

Table 9: Prompt setting used for GRPO training. The text description and assistant output shown are examples; actual inputs and outputs vary by sample.

Prompt for Bounding Box Prediction
<p>System Message:</p> <p>Task Definition:</p> <ul style="list-style-type: none"> You are a remote sensing image understanding and reasoning assistant. Your task is to locate the target object in the image based on the provided text description and output its bounding box coordinates. Please follow these requirements: <ol style="list-style-type: none"> Text comprehension: <ul style="list-style-type: none"> Carefully analyze the text description to identify the target object. Output format: <ul style="list-style-type: none"> If one object exists: Output the bounding box coordinates in the format: [x_min, y_min, x_max, y_max]. If no matching object is found: Output an empty list []. If multi-objects exist: Output the bounding box coordinates in the format: [[x_min1, y_min1, x_max1, y_max1], [x_min2, y_min2, x_max2, y_max2], ...]. Coordinate requirements: <ul style="list-style-type: none"> Coordinate values must be integers representing pixel positions. Critical: You MUST output the tight bounding box around the object. Output specifications: <ul style="list-style-type: none"> Output the thinking process in <think> </think> and final answer (a list of bbox) in <answer> </answer> tags. <p>Task Input:</p> <p>Perform the detection task for the following input:</p> <p><image></p> <p>Text description: (A natural language instruction describing the target object.)</p> <hr/> <p>User:</p> <ul style="list-style-type: none"> Text description: <p>"What specific area is allocated for the vertical lift and descent of helicopters and similar rotary-wing vehicles?" (This is an example question. Actual descriptions should be adapted to specific task needs.)</p> <hr/> <p>Assistant:</p> <ul style="list-style-type: none"> Reasoning Process: <p><think> The airport helipad is a designated area for safe helicopter landings and departures, clearly marked to ensure exclusively secure operations for aerial vehicles. </think></p> Bounding Box Output: <p><answer> [[500, 164, 605, 246], [404, 320, 516, 404]] </answer></p>